

Analyzing π^0 photoproduction data on the proton at energies of 1.5–2.3 GeV

K. Nakayama^{1,2} and H. Haberzettl^{3,2}

¹Department of Physics and Astronomy, University of Georgia, Athens, GA 30602, USA

²Institut für Kernphysik (Theorie), Forschungszentrum Jülich, D-52425 Jülich, Germany

³Center for Nuclear Studies, Department of Physics,
The George Washington University, Washington, DC 20052, USA

(Dated: 18 July 2005)

The recent high-precision data for the reaction $p + p \rightarrow \pi^0$ at photon energies in the range 1.5–2.3 GeV obtained by the CLAS collaboration at the Jefferson Laboratory have been analyzed within an extended version of the photoproduction model developed previously by the authors based on a relativistic meson-exchange model of hadronic interactions [Phys. Rev. C 69, 065212 (2004)]. The π^0 photoproduction can be described quite well over the entire energy range of available data by considering S_{11} , P_{11} , P_{13} , and D_{13} resonances, in addition to the t-channel mesonic currents. The observed angular distribution is due to the interference between the t-channel and the nucleon s- and u-channel resonance contributions. The $j = 3/2$ resonances are required to reproduce some of the details of the measured angular distribution. For the resonances considered, our analysis yields mass values compatible with those advocated by the Particle Data Group. We emphasize, however, that cross-section data alone are unable to pin down the resonance parameters and it is shown that the beam and/or target asymmetries impose more stringent constraints on these parameter values. It is found that the nucleonic current is relatively small and that the $N N^0$ coupling constant is not expected to be much larger than 2.

PACS numbers: 25.20.Lj, 13.60.Le, 13.75.-n, 14.20.Gk

I. INTRODUCTION

One of the primary interests in investigating the π^0 photoproduction reaction is that it may be suited to extract information on nucleon resonances, N^0 , in the less explored higher N^0 mass region. Current knowledge of most of the nucleon resonances is mainly due to the study of N^0 scattering and/or pion photoproduction off the nucleon. Since the π^0 meson is much heavier than a pion,

π^0 meson-production processes near threshold necessarily sample a much higher resonance-mass region than the corresponding pion production processes. They are well-suited, therefore, for investigating high-mass resonances in low partial-wave states. Furthermore, reaction processes such as π^0 photoproduction provide opportunities to study those resonances that couple only weakly to pions, in particular, those referred to as "missing resonances", which are predicted by quark models, but not found in more traditional pion-production reactions [1].

Another special interest in π^0 photoproduction is the possibility to impose a more stringent constraint on its yet poorly known coupling strength to the nucleon. This has attracted much attention in connection with the so-called "nucleon-spin crisis" in polarized deep inelastic lepton scattering [2]. In the zero-squared-momentum limit, the $N N^0$ coupling constant $g_{NN^0}(q^2 = 0)$ is related to the avor singlet axial charge G_A through the avor singlet Goldberger-Treiman relation [3] (see also Refs. [4, 5])

$$2m_N G_A(0) = F g_{NN^0}(0) + \frac{F^2}{2N_F} m^2 g_{NNG}(0); \quad (1)$$

where F is a renormalization-group invariant decay con-

stant defined in Ref. [3], N_F is the number of flavors, and m_N and m^0 are the nucleon and π^0 masses, respectively; g_{NNG} describes the coupling of the nucleon to the gluons arising from contributions violating the Okubo-Zweig-Iizuka rule [6]. The EMC collaboration [2] has measured an unexpectedly small value of $G_A(0) = 0.20 \pm 0.35$. The first term on the right-hand side of the above equation corresponds to the quark contribution to the "spin" of the proton, and the second term to the gluon contribution [5, 7]. Therefore, once $g_{NN^0}(0)$ is known, Eq. (1) may be used to extract the coupling $g_{NNG}(0)$. Unfortunately, however, there is no direct experimental measurement of $g_{NN^0}(0)$ so far. Reaction processes where the π^0 meson is produced directly off a nucleon may thus offer a unique opportunity to extract this coupling constant. Here it should be emphasized that, as has been pointed out in Ref. [8], hadronic model calculations such as the present one cannot determine the $N N^0$ coupling constant in a model-independent way. At best, we get an estimate for the range of its value at the on-shell kinematic point, i.e., at $q^2 = m^2$. Assuming the usual behavior of hadronic form factors for off-shell mesons which generally decrease for $q^2 < m^2$, we expect then that an eventually small upper limit of $g_{NN^0}(q^2 = m^2)$ would lead to an even smaller value of $g_{NN^0}(0)$, which is needed in Eq. (1) to extract $g_{NNG}(0)$.

The main purpose of the present work is to perform an analysis of the $p + p \rightarrow \pi^0$ reaction within an extended version of the relativistic meson-exchange model of hadronic interactions as reported in Ref. [8]. This analysis is motivated by the new high-precision cross-section data obtained by the CLAS collaboration [9] at the Jefferson Laboratory (JLab). The new data supersede the previous

SAPHIR data [10] analyzed in Ref. [8] both in absolute normalization and angular shape.

The present paper is organized as follows. In Sec. II the extension of our model [8] for $p \rightarrow p^0$ is given. The results of the corresponding model calculations are presented in Sec. III. Section IV contains a summary with our conclusions. Some technical details of the present model are given in the Appendix.

II. FORMALISM

The dynamical content of the present $p \rightarrow p^0$ photoproduction calculation is summarized by the graphs of Fig. 1 where we employ form factors at the vertices to account for the hadronic structure. The gauge invariance of this production current is ensured by a phenomenological contact current, according to the prescription of Refs. [11–13]. This contact term provides a rough phenomenological description of the final-state interaction which is not treated explicitly here. The basic details of the present approach are the same as in our previous paper [8] and we will not repeat them here. There are, however, a few modifications and improvements and those will be discussed here.

A. Spin-3/2 resonances

The present fits also require the inclusion of spin-3/2 resonances, denoted generically by N^0 . The Lagrangian for the hadronic $N N^0$ interaction is given by

$$L_{NN^0}^{(+)} = \frac{g_{NN^0}}{m_0} N^0 \quad (z) \quad (+) N @ 0 + H.c.; \quad (2)$$

where N^0 , N , and 0 are the resonance, nucleon, and meson fields, respectively, and

$$(+)_5 = 1 \quad \text{and} \quad (-)_5 = 1 \quad (3)$$

pertain to positive- and negative-parity resonances, respectively. For the coupling tensor, $g = g(z)$, we take $z = \frac{1}{2}$ for the on-shell parameter for simplicity. The Lagrangian for the electromagnetic transition current reads

$$L_{NN^0} = ie \frac{g_{1NN^0}}{m_N} N^0 \gamma_5 N F + e \frac{g_{2NN^0}}{2m_N^2} \partial N^0 \gamma_5 N F + H.c.; \quad (4)$$

where $F = \partial A \cdot \partial A$ is the electromagnetic field-strength tensor (with A being the vector potential).

B. Energy-dependent resonance widths

For the present application, we have adapted our formalism to accommodate energy-dependent resonance widths with the appropriate threshold behavior.

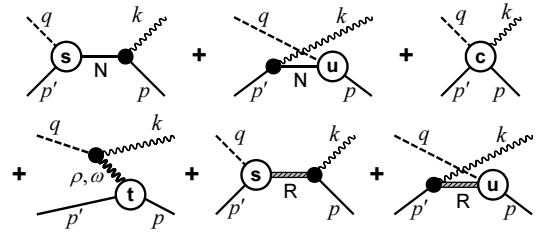


FIG. 1: Diagrams contributing to $p \rightarrow p^0$. The process proceeds from right to left. The intermediate baryon states are denoted N for the nucleon, and R for the S_{11} , P_{11} , P_{13} , and D_{13} resonances. The intermediate mesons in the t -channel are π and ρ . The external legs are labeled by the four-momenta of the respective particles and the labels s , u , and t of the hadronic vertices correspond to the on-shell Mandelstam variables of the respective intermediate particles. The three diagrams in the lower part of the diagram are transverse individually; the three diagrams in the upper part are made gauge-invariant by an appropriate choice for the contact current depicted in the top-right diagram. The nucleonic current (nuc) referred to in the text corresponds to the top line of diagram s ; the meson-exchange current (mc) and resonance current contributions correspond, respectively, to the leftmost diagram and the two diagrams on the right of the bottom line of diagram s .

For a spin-1/2 resonance propagator, we use the ansatz

$$S_{1=2}(p) = \frac{1}{p - m_R + \frac{i}{2}} = \frac{p + m_R}{p^2 - m_R^2 + \frac{1}{2}(p + m_R)}; \quad (5)$$

where m_R is the mass of the resonance with four-momentum p . Γ is the width function whose functional behavior will be given below.

For spin-3/2, the resonant propagator reads in a schematic matrix notation

$$S_{3=2}(p) = (p - m_R)g \quad \frac{i}{2} \quad : \quad (6)$$

All indices are suppressed here, i.e., g is the metric tensor and Γ is the Rarita-Schwinger tensor written in full detail as

$$= g + \frac{1}{3} \Gamma^{\mu\nu\alpha\beta} + \frac{2p^\mu p^\nu}{3m_R^2} + \frac{p^\mu p^\nu}{3m_R}; \quad (7)$$

where μ , ν , and α enumerate the four indices of the 3×3 matrix components (summation over α is implied). The inversion in (6) is to be understood on the full 16-dimensional space of the four Lorentz indices and the four components of the gamma matrices. The motivation for the ansatz (6) and the technical details how to perform this inversion is given in the Appendix.

In both cases, we write the width Γ as a function of $W = \sqrt{p^2}$ according to

$$(W) = \sum_{i=1}^2 \frac{X^i}{R^4} \hat{i}_i(W) + \sum_{j=1}^5 \frac{X^j}{R^4} \hat{j}_j(W); \quad (8)$$

where the sum s over i and j respectively account for decays of the resonance into N two- or three-hadron channels and into N radiative decay channels. The total static resonance width is denoted by W_R and the numerical factors i and j (with $0 \leq i, j \leq 1$) describe the branching ratios into the various decay channels, i.e.,

$$\sum_{i=1}^N \sum_{j=1}^N i + j = 1 : \quad (9)$$

Similar to Refs. [14–17], we parameterize the width functions $\hat{\gamma}_i$ and $\hat{\gamma}_j$ (which are both normalized to unity at $W = m_R$) to provide the correct respective threshold behaviors.

For the decay of the resonance into two hadronic fragments with masses m_{i1} and m_{i2} , the hadronic width functions $\hat{\gamma}_i$ are taken as

$$\hat{\gamma}_i(W) = \frac{q_i}{q_{iR}} \frac{2L+1}{\frac{2}{i} + \frac{q_{iR}^2}{q_i^2}} D_i(W) \quad (10)$$

for $W > m_{i1} + m_{i2}$, and zero otherwise. L denotes the partial wave in which the resonance is found and the momentum q_i is the magnitude of the center-of-mass momentum three-momentum of the two fragments, i.e.,

$$\hat{\gamma}_i(W) = \frac{p}{2W} \frac{[W^2 - (m_{i1} + m_{i2})^2]W^2 - (m_{i1} - m_{i2})^2}{(m_{i1} + m_{i2})^2} \quad (11)$$

and $q_{iR} = q_i(m_R)$. For the decay of the resonance into one baryon and two mesons (for example, N^0), we use

$$\hat{\gamma}_i(W) = \frac{q_i}{q_{iR}} \frac{2L+4}{\frac{2}{i} + \frac{q_{iR}^2}{q_i^2}} D_i(W) ; \quad (12)$$

where m_{i2} in (11) needs to be replaced by the sum of the two meson masses for this case, and m_{i1} is the baryon mass. In principle, the factor

$$D_i(W) = \frac{m_R}{W}^{n_i} ; \quad \text{with } n_i \geq 0 ; \quad (13)$$

allows for a modification of the asymptotic behavior of $\hat{\gamma}_i(W)$, however, we use $n_i = 0$ throughout for simplicity. The parameter i is an inverse range parameter; since we found very little sensitivity to varying this parameter (within reasonable ranges), we kept it fixed at $i = 1 \text{ fm}^{-1}$ for all channels.

The width function $\hat{\gamma}_j$ for the decay into a hadron with mass m_j and a photon with three-momentum k_j is taken as

$$\hat{\gamma}_j(W) = \frac{k_j}{k_{jR}} \frac{2L+2}{\frac{2}{j} + \frac{k_{jR}^2}{k_j^2}} D_j(W) ; \quad (14)$$

where

$$k_j(W) = \frac{W^2 - m_j^2}{2W} \quad (15)$$

for $W > m_j$, and zero otherwise, and $k_{jR} = k_j(m_R)$. As in the hadronic case, the asymptotic damping function is given by

$$D_j(W) = \frac{m_R}{W}^{r_j} ; \quad \text{with } r_j \geq 0 ; \quad (16)$$

Again, for simplicity, we employ $r_j = 0$ throughout. In practice, for the present case, the photon decay channels are negligibly small and play no role for the total width. The corresponding branching ratio $\hat{\gamma}_N$ for the N channel is only needed to extract the value of the N^0 branching ratio $\hat{\gamma}_N$ (see below).

III. RESULTS AND DISCUSSION

Before we discuss the details of our results, some general remarks are in order. The basic strategy of our model approach is to start with the nucleon plus meson-exchange currents and add the resonances one by one as needed in the fitting procedure until one achieves a reasonable t of the new N^0 photoproduction data obtained by the CLAS collaboration [9]. We allow for both spin-1/2 and -3/2 resonances in our model. Our quantitative criterion for a reasonable t was to discard all t s with a t^2 per data point of $t^2 = N > 4$, which is supported by the fact that t s with $t^2 = N$ much larger than 4 are noticeably of inferior t quality even for the naked eye. Under this criterion, we found that one needs about five resonances in order to obtain a reasonable t in the present approach. We find, in particular, that, in addition to spin-1/2 resonances, spin-3/2 resonances are necessary to achieve acceptable t s.

As we have pointed out in Ref. [8], the cross-section data alone are unable to pin down the model parameters and, therefore, one finds different sets of parameters which fit the data equally well. Note that this is not due to the uncertainties in the data, but simply because, intrinsically, the cross sections do not impose enough stringent constraints on the t . In particular, for each resonance, the resulting fitted mass value depends to a certain extent on its starting value in the fitting procedure. The starting (resonance) mass values we consider here generally are around those advocated by the Particle Data Group (PDG) [18].

In the present work, in the case of those resonances that can be identified with known PDG resonances, we have taken into account only the corresponding dominant branching ratios i from the PDG for hadronic decays when this information is available (and we ignored the fact that some of the quoted branching ratios are subject to large uncertainties). If no information is available, we consider only the N partial decay, with the corresponding branching ratio $\hat{\gamma}_N$ as a free parameter. Apart from these branching ratios, we also consider the N^0 branching ratio $\hat{\gamma}_N$ which is calculated from the product of the coupling constants $g_{NN} \cdot g_{NN}$ in conjunction with the assumed branching ratio $\hat{\gamma}_N$ for

the radiative decay. In the following tables, therefore, η^0 is not an independent t parameter, but rather a parameter extracted from the fitted values of the product $g_{NN}^0 g_{NN}$.

One might expect that the way in which the energy dependence is implemented in the resonance width in the present work [cf. Eqs. (12)–(14)] may introduce a considerable uncertainty in the final results. However, we find that the cross sections are not very sensitive to our assumptions in this respect. In fact, we also re-ran some of the cross-section fits discussed below using step functions for the widths that switch on the full partial widths at the corresponding thresholds without any smooth energy dependence and we found that the parameter sets obtained in this way were fairly close to the ones reported here. For spin observables, however, this insensitivity does not hold true. In particular, the beam and target asymmetries are rather sensitive to how the energy dependence of the width is treated and one must be careful then when confronting model predictions with the data when the latter should become available.

We now turn to the discussion of the details of our analysis. We emphasize that the results shown here do not necessarily have the lowest χ^2 . Rather, they are sample fits that illustrate the different dynamical features one may obtain considering only the currently available data in the analysis within the t -quality criteria mentioned above. We would like to point out, however, that we could not obtain t qualities much better than $\chi^2/N = 3.5$. The major reason for this relatively large value is that the CLAS data [9] have very small error bars and as a consequence deviations of the fits from some of the more detailed features of the data lead to considerable increases in χ^2 . The data and our fits are summarized in Fig. 2. Of particular relevance for χ^2 increases are the details of the angular distributions at incident photon energies $T = 1.728$ and 2.079 GeV. The data, furthermore, seem to indicate a rather strong change in the angular distributions from $T = 1.527$ to 1.577 GeV, a feature which cannot be reproduced easily. Of course, whether these features are actually present in the data or simply statistical fluctuations not accounted for in the quoted error bars remains to be confirmed.

A. Differential cross sections

The details of the fits presented here are given in Tables I–IV and the corresponding Figs. 3–6. For the purpose of easy comparison, Fig. 2 provides an overview of all those results. All four fits were obtained using the energy-dependent width functions of Sec. II B and have comparable overall χ^2/N values. We see that most of the differences among them are at forward angles where there are no data. Despite the fact that the overall quality of the fits is comparable, the resulting parameter values are quite different. In particular, all the resonances in Table I are above the η^0 production thresh-

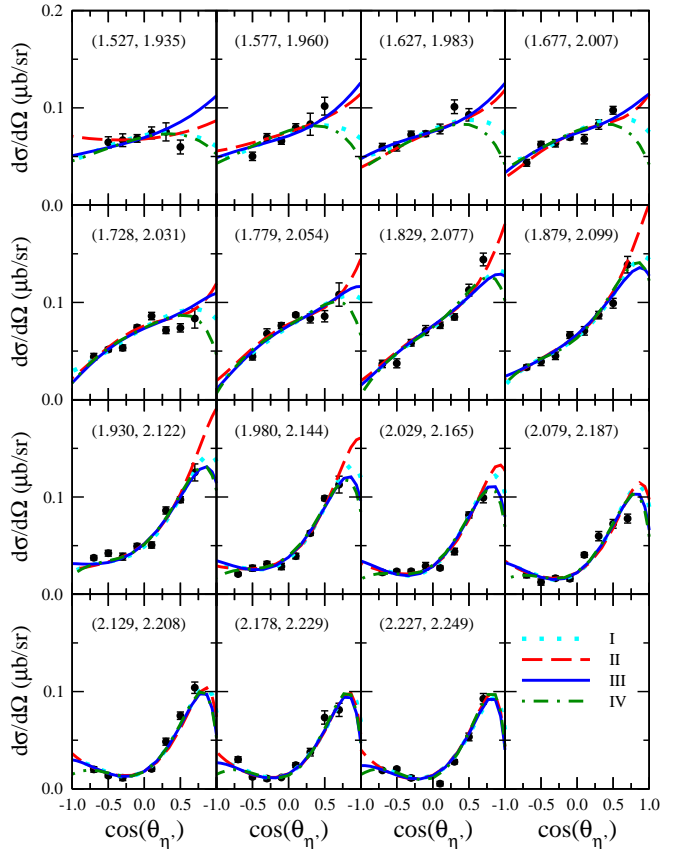


FIG. 2: (Color online) Differential cross section for $p^+ p^0$ according to the mechanisms shown in Fig. 1 as a function of the η^0 emission angle θ in the center-of-mass frame of the system. As indicated in the legend, the curves correspond to the fits results of Tables I (dotted lines), II (dashed), III (solid), and IV (dash-dotted). The numbers (T ; W) in parentheses are the incident photon energy T and the corresponding s -channel energy $W = \sqrt{s}$, respectively, in GeV. The data are from Ref. [9].

old energy. As mentioned before, although we cannot identify the resonances uniquely in the present analysis, Table I reveals that two of the resulting spin-3/2 resonances, $P_{13}(1900)$ and $D_{13}(2084)$, are consistent with those seen and quoted by the PDG [18] as two-star resonances. Also, in this particular set of parameters, the resulting $N N^0$ coupling constant is consistent with zero. The fit set of Table II includes three S_{11} and three P_{11} resonances, instead of one each as in Table I, keeping the number of spin-3/2 resonances unchanged. Here, two of the S_{11} , one of the P_{11} and one of the D_{13} resonances end up well below the production threshold, while one P_{11} resonance mass is close to 2.5 GeV. With the exception of the latter resonance, all the resulting resonance masses are consistent with those quoted by the PDG [18] as four-star [$S_{11}(1535)$, $S_{11}(1650)$], three-star [$P_{11}(1710)$; $D_{13}(1720)$], two-star [$P_{13}(1900)$, $D_{13}(2080)$], and one-star [$S_{11}(2090)$; $P_{11}(2100)$] resonances. Here, the $N N^0$ coupling constant is $g_{NN}^0 = 15$. In the

TABLE I: Model parameters fitted to the $p + {}^0p$. (See text, and also Ref. [8], for explanations of parameters.) Values in boldface are not fitted. The branching ratios g_{NN^0} are assumptions made to extract g_{NN^0} (for the total width, however, the g_{NN^0} values are too small to be relevant). The starting values for fitting all resonance masses were chosen here within the energy range covered by the data set. $^2=N=372$.

Nucleonic current:			
g_{NN^0}	0.01		
	0.0		
m_N (MeV)	1200		
Mesonic current:			
g_0	1.25		
$g_{0!}$	0.44		
m_N (MeV)	1288		
$N = S_{11}$ current:			
m_N (MeV)	1913		
g_{NN^0}	0.21		
	1.00		
m_N (MeV)	1200		
m_N (MeV)	57		
g_N	0.002		
g_N	0.03		
g_{N^0}	0.97		
$N = P_{11}$ current:			
m_N (MeV)	1994		
g_{NN^0}	-1.64		
	0.01		
m_N (MeV)	1200		
m_N (MeV)	148		
g_N	0.002		
g_N	0.35		
g_{N^0}	0.65		
$N = P_{13}$ current:			
m_N (MeV)	1900		
g_{NN^0}	-0.06		
g_{2NN^0}	-0.08		
m_N (MeV)	1200		
m_N (MeV)	109		
g_N	0.002		
g_N	0.60		
$g_{N!}$	0.4		
g_{N^0}	0.00		
$N = D_{13}$ current:			
m_N (MeV)	1909	2084	
g_{NN^0}	1.16	0.14	
g_{2NN^0}	0.47	0.18	
m_N (MeV)	1200	1200	
m_N (MeV)	289	124	
g_N	0.002	0.002	
g_N	1.00	0.95	
g_{N^0}	0.00	0.05	

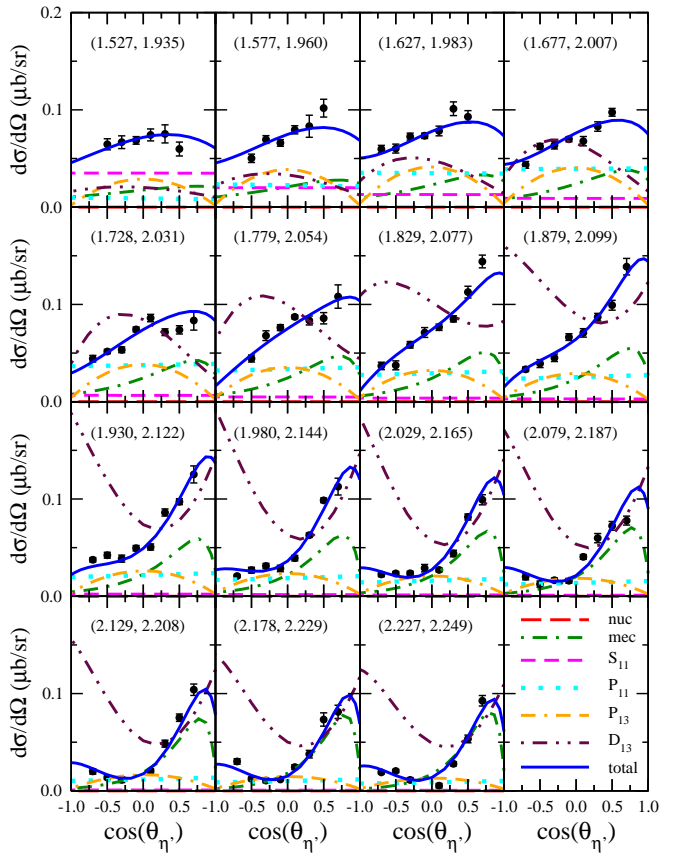


FIG. 3: (Color online) Differential cross sections and the dynamical content of the present model corresponding to the fit result of Table I. The dash-dotted curves correspond to the mesonic current contribution; the dashed curves to the S_{11} resonance current and the dotted curves to the P_{11} resonance. The dot-double-dashed curves correspond to the P_{13} resonance current while the dash-double-dotted curves show the D_{13} resonance contribution. The solid curves correspond to the total current. The nucleonic current contribution (long-dashed curves) are negligible and cannot be seen on the present scale.

fit result of Table III, we have omitted the P_{13} resonance and considered two S_{11} , three P_{11} and two D_{13} resonances. Again, three of the resulting resonances, S_{11} (1538), P_{11} (1710), and D_{13} (2090), are consistent with the known resonances. The $N N^0$ coupling constant is practically zero, in line with the fit result of Table I. We have also considered all the known spin-1/2 and -3/2 resonances [18] (including those with only one star) in our fit.¹ The resulting parameter values are displayed in Table IV. Here the resonance masses are fixed at the respective (centroid) values given in Ref. [18]. The resulting resonance widths are all consistent with those quoted

¹ There are also established spin-5/2, -7/2, and -9/2 resonances [18] in the energy region covered by the JLab data, but they have been omitted in the present analysis.

TABLE II: Same as Table I. More resonances were added here to see whether this would improve the t . $t^2 = 3.85$.

Nucleonic current:			
g_{NN^0}	1.49		
	0.0		
m_N (MeV)	1200		
Mesonic current:			
g_0^0	1.25		
g_0^1	0.44		
m_ν (MeV)	1508		
$N = S_{11}$ current:			
m_N (MeV)	1535	1626	2082
g_{NN^0}	-6.04	0.46	0.01
	0.89	0.79	0.97
m_N (MeV)	1200	1200	1200
m_N (MeV)	180	141	142
m_N		0.001	
m_N	0.5	0.9	1.00
m_N	0.5	0.1	
m_N^0		0.00	
$N = P_{11}$ current:			
m_N (MeV)	1712	2094	2474
g_{NN^0}	1.41	-0.58	-0.49
	0.96	0.94	0.76
m_N (MeV)	1200	1200	1200
m_N (MeV)	73	145	173
m_N		0.002	0.002
m_N	0.15	0.72	0.02
m_N	0.85		
m_N^0		0.28	0.98
$N = P_{13}$ current:			
m_N (MeV)	1941		
g_{1NN^0}	g_{NN^0}	0.10	
g_{2NN^0}	g_{NN^0}	-0.12	
m_N (MeV)	1200		
m_N (MeV)	136		
m_N	0.58		
m_N^1	0.4		
m_N^0	0.02		
$N = D_{13}$ current:			
m_N (MeV)	1726	2092	
g_{1NN^0}	g_{NN^0}	0.17	0.01
g_{2NN^0}	g_{NN^0}	-0.24	0.11
m_N (MeV)	1200	1200	
m_N (MeV)	104	146	
m_N		0.001	
m_N	0.1	0.93	
m_N	0.9		
m_N^0		0.07	

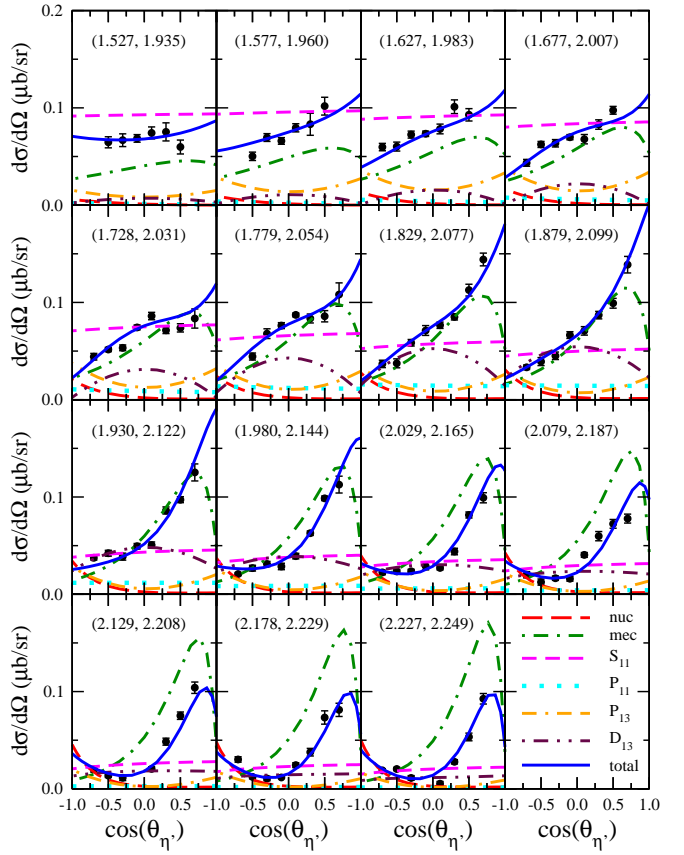


FIG. 4: (Color online) Same as in Fig. 3 for the t result of Table II.

in Ref. [18]. For the NN^0 coupling constant, we obtained $g_{NN^0} = 1.12$.

All these parameter sets illustrate the fact that cross sections do not impose enough constraints to the t in order to extract definitive information on the resonances. Spin observables, on the other hand, do impose more stringent constraints and help distinguish among these parameter sets, as we shall show later.

Although the parameter sets in Tables I-IV yield comparable fits to the cross section, the corresponding dynamical contents are quite different from each other. Let us discuss, therefore, some of the different features present in the results corresponding to the various parameter sets. Figure 3 shows some details of the dynamical content of our model corresponding to the t results given in Table I. At the lowest energy measurement, the S_{11} resonance contribution is the largest, but already around $T = 1.779$ GeV, it becomes very small and it is practically negligible for higher energies. The P_{11} resonance contribution reaches its maximum around $T = 1.728$ GeV. Its angular shape is rather flat (note that it includes both the s- and u-channel contributions). However, its interference with other contributions, such as that due to the S_{11} resonance, leads to a distinctive angular dependence. The P_{13} resonance contribution is relatively large especially in the low energy region and it

TABLE III: Same as Table I. No P_{13} resonance was allowed here. $^2N = 382$.

Nucleonic current:			
g_{NN^0}	0.00		
	0.0		
N (MeV)	1200		
Mesonic current:			
g_0	1.25		
g_{01}	0.44		
v (MeV)	1402		
$N = S_{11}$ current:			
m_N (MeV)	1538	1846	
g_{NN^0}	-10.57	2.23	
	1.00	1.00	
N (MeV)	1200	1200	
N (MeV)	234	171	
N	0.5	1.00	
N	0.5		
$N = P_{11}$ current:			
m_N (MeV)	1710	2002	
g_{NN^0}	4.69	-1.64	
	1.00	0.00	
N (MeV)	1200	1200	
N (MeV)	187	138	
N	0.002		
N	0.15	0.15	
N	0.85		
N^0	0.85		
$N = D_{13}$ current:			
m_N (MeV)	1814	2090	
g_{1NN^0}	0.55	0.11	
g_{2NN^0}	0.01	0.17	
N (MeV)	1200	1200	
N (MeV)	89	139	
N	0.002		
N	1.00	0.96	
N^0	0.04		

peaks around $T = 1.627$ GeV. Its angular shape is concave with a maximum at $\theta = 90^\circ$. The D_{13} resonance contribution is large over the energy region considered, except at lower energies. Above $T = 1.728$ GeV, it is the largest contribution. Its angular shape changes drastically with energy, starting with a small negative curvature in the lower energy region and ending with a roughly convex shape in the higher energy region. Note that this energy dependence of the angular shape is due to an interference between the two D_{13} resonances with different masses. We found that it requires at least two D_{13} resonances to achieve a reasonable fit. The mesonic current contribution plays a crucial role in reproducing the observed forward-peaked angular distribution at higher

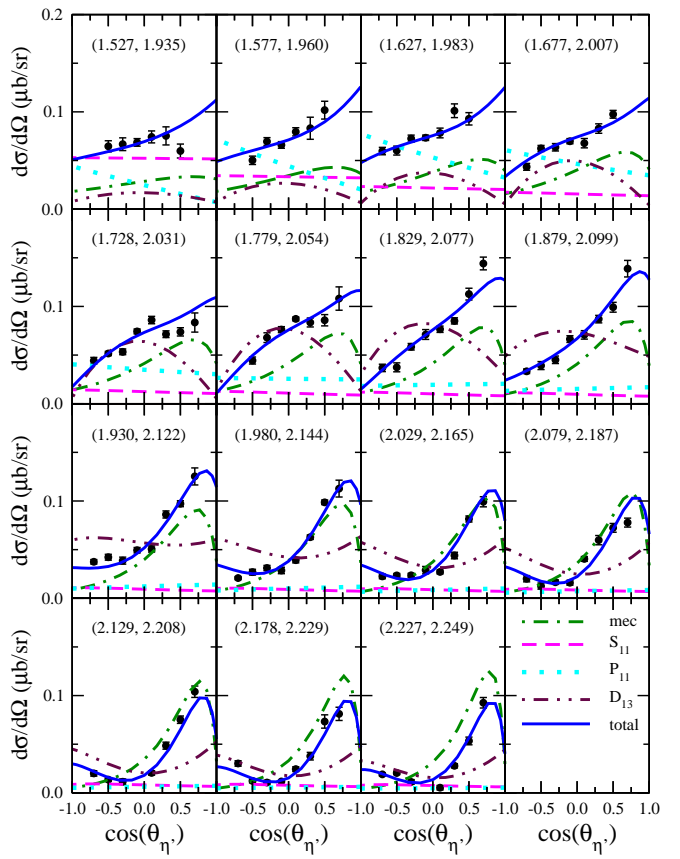


FIG. 5: (Color online) Same as in Fig. 3 for the t result of Table III.

energies. This is a general feature observed in many reactions at high energies where the t -channel mechanism (either Regge trajectories or meson exchanges) accounts for the small behavior of the cross section. However, the present result shows also a competing mechanism due to resonances (especially the D_{13} resonance) and that the observed forward-peaked angular distribution is a result of significant interference effects. We note that this feature is not restricted to the particular set of the parameter values of Table I, but it is also found in other sets that fit the data, as one can see in Figs. 4–6. Therefore, this feature prevents us from fixing uniquely the mesonic current from the cross-section data at forward angles and higher energies. The nucleonic current is practically zero in Fig. 3 since, as mentioned above, the resulting NN^0 coupling constant is negligibly small. However, as mentioned in the beginning of this section, the cross-section data alone do not impose stringent constraints on the t so that it is possible to reproduce the data equally well with a larger coupling constant, as can be seen in Tables II and IV. We will come back to this issue later, in Sec. III C.

In the t result of Table II shown in Fig. 4, the S_{11} resonance contribution is very strong especially in the lower energy region and is quite appreciable even at higher energies. The P_{11} resonance contribution is relatively small

TABLE IV : Same as Table I. All resonance masses are kept at their PDG values. $^2=N = 355$.

Nucleonic current:			
g_{NN^0}	1.12		
	0.0		
N (MeV)	1200		
Mesonic current:			
g_0	1.25		
g_{01}	0.44		
ν (MeV)	1422		
$N = S_{11}$ current:			
m_N (MeV)	1535	1650	2090
g_{NN^0}	-9.03	7.09	-0.09
	0.35	0.25	1.00
N (MeV)	1200	1200	1200
N (MeV)	111	197	73
N		0.001	
N	0.5	0.9	0.06
N	0.5	0.1	
N^0		0.94	
$N = P_{11}$ current:			
m_N (MeV)	1440	1710	2100
g_{NN^0}	-1.11	-3.35	-0.49
	1.00	0.09	0.08
N (MeV)	1200	1200	1200
N (MeV)	256	121	87
N		0.002	
N	0.65	0.15	0.43
N	0.35	0.85	
N^0		0.57	
$N = P_{13}$ current:			
m_N (MeV)	1720	1900	
g_{1NN^0}	-0.56	0.11	
g_{2NN^0}	1.63	-0.62	
N (MeV)	1200	1200	
N (MeV)	103	345	
N	0.2	0.6	
N	0.8		
N^0		0.4	
$N = D_{13}$ current:			
m_N (MeV)	1520	1700	2080
g_{1NN^0}	0.37	1.17	0.05
g_{2NN^0}	0.65	0.91	0.07
N (MeV)	1200	1200	1200
N (MeV)	110	49	112
N		0.001	
N	0.55	0.10	0.98
N	0.45	0.90	
N^0		0.02	

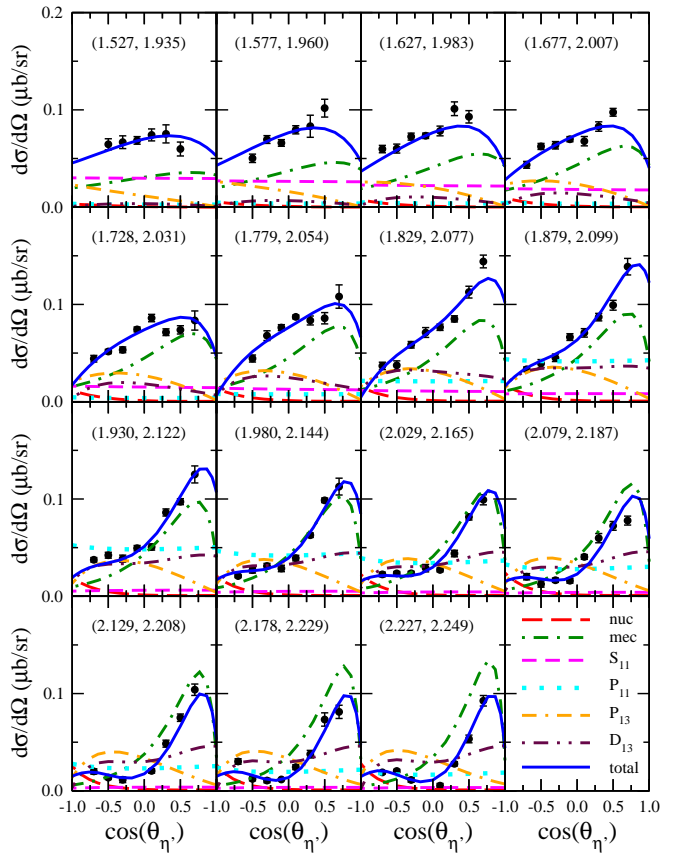


FIG. 6: (Color online) Same as in Fig. 3 for the t result of Table IV.

by itself but cannot be ignored because of the interference with other currents. The P_{13} resonance contribution basically shows the same overall energy dependence as in the t sets discussed above, except that the shape of the angular distribution in this case is convex instead of concave. This difference is due to the relative sign difference between the coupling constants g_{1NN^0} and g_{2NN^0} as compared to the t result of Table I shown in Fig. 3. The D_{13} resonance contribution is largest around $T = 1.829$ GeV. The shape of the angular distribution is quite different from the other t discussed above. Together with the P_{13} resonance, it describes some of the details of the observed angular distribution around $T = 1.779$ GeV. The mesonic current is much larger in this t than in the other t s. In particular, it largely overestimates the measured cross section in the higher energy region. Its destructive interference with the other currents brings down the total contribution in agreement with the data. Moreover, this shows that one has to be cautious in trying to fit the t -channel contribution using the cross-section data at forward angles and higher energies. The nucleonic current gives an appreciable contribution in this t , especially at higher energies and backward angles due to the u -channel. The corresponding N^0 coupling constant is $g_{NN^0} = 1.49$.

Figure 5 shows the dynamical content of the t re-

sult of Table III. The S_{11} resonance contribution is largest at the lowest energy, but it decreases quickly as the energy increases. The P_{11} resonance contribution is largest around $T = 1.627$ GeV, with more pronounced angular distribution than in the other t results. The D_{13} resonance contribution has a concave angular shape in the lower energy region and is largest at around $T = 1.829$ GeV. For higher energies the angular shape changes and gives the largest contribution for forward angles apart from the mesonic current, the latter providing again the bulk of the observed rise of the cross section at forward angles. The P_{13} resonance is not included in this t set. We note that, unlike in Fig. 4, some of the details of the observed angular distribution around $T = 1.779$ GeV is not well reproduced, indicating the importance of both the P_{13} and D_{13} resonances. The nucleonic current contribution is practically zero.

The dynamical content of the t result given in Table IV is shown in Fig. 6. Overall, except for the lowest energy, the mesonic current yields the largest contribution. The S_{11} and P_{13} resonance contributions are important in the low energy region while the P_{11} , P_{13} , and D_{13} resonances are important in the higher energy region. The nucleonic current is non-negligible only for backward angles at higher energies. Here, one major difference from the other t results is the rather pronounced bending downward of the cross section (solid curves) for forward angles at lower energies. Measurements of the cross sections for more forward angles would tell us whether such a behavior would indeed be necessary.

B. Total cross sections

Figure 7 shows the predictions for the total cross sections obtained by integrating the corresponding differential cross sections shown in Figs. 3–6. Although these predictions may suffer from considerable uncertainties due to differences in the corresponding differential cross sections, they exhibit a common feature, i.e., the total cross sections (solid curves) seem to show a bump structure around $W = 2.09$ GeV which is caused mainly by the D_{13} resonance. In the result corresponding to Table IV (bottom panel), the P_{11} also contributes to this bump structure. Note that for this case both the D_{13} (2080) and P_{11} (2100) resonances coincide at this bump position thus making it more prominent. There is also a one-star resonance, S_{11} (2090), that is just at the bump and, therefore, might have contributed to its structure. However, the angular distribution does not favor this possibility. The total cross section also seems to exhibit a bump structure at a lower energy of around $W = 1.96$ GeV due to, dominantly, the S_{11} resonance which causes a rather sharp rise of the cross section from the threshold. The P_{13} and P_{11} resonances can also contribute to the broadening of this bump depending on the t set, as can be seen in Fig. 7. The structures exhibited by the total cross section are unlikely to be artifacts of the present predictions and,

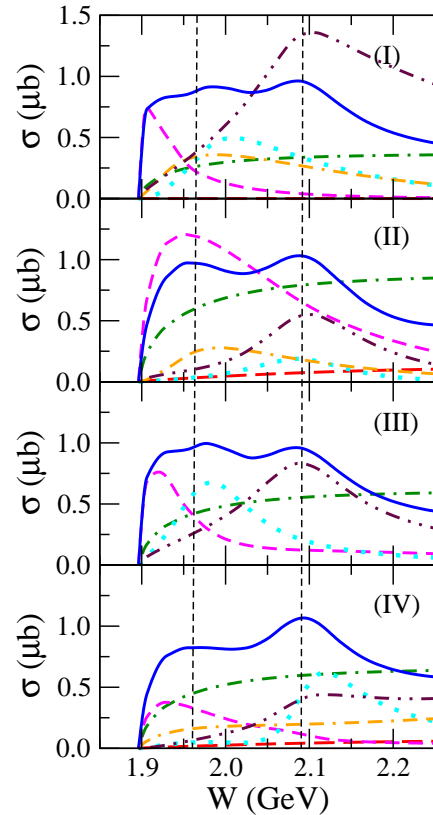


FIG. 7: (Color online) Total cross section for $p + p \rightarrow p + p^0$ as a function of the total energy of the system, $W = p_s$. As indicated in the legend, the panels correspond to the t results of Tables I (top panel), II (upper-middle), III (lower-middle), and IV (bottom). The overall total cross sections (solid lines) are broken down according to their dynamical contributions, with line styles defined in Fig. 3. The two dashed vertical lines are placed to guide the eye through the two bump positions in all panels.

consequently, we would expect them to show up in the actual total cross-section data when they are measured. However, if this is indeed the case, the question whether such features are actually due to nucleon resonances (as in the present study) remains to be corroborated.

C. $N N^0$ coupling constant

As we have seen in this section, unfortunately the present analysis cannot determine the $N N^0$ coupling constant, since the available cross-section data can be reproduced equally well with different sets of parameters in which this coupling constant varies considerably. However, an upper limit of its value can still be estimated. One of the reasons why g_{NN^0} cannot be extracted uniquely from the cross-section data is that the resonance currents, especially the one due to the D_{13} resonance, can give rise to the observed enhancement of the backward-angle cross section as shown in Figs. 3–6. Also,

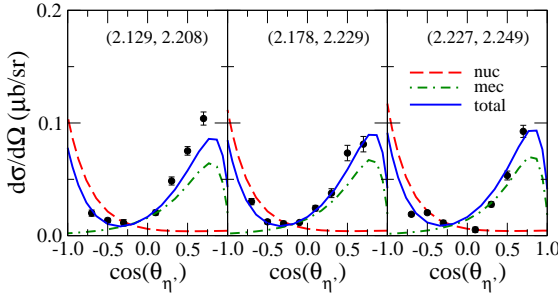


FIG. 8: (Color online) Fit result with no resonances. $g_{NN} = 2.28$ and $v = 1257$ MeV. See caption of Fig. 3.

the P_{11} resonance current alone can lead to a feature of the cross section similar to that due to the nucleonic current, i.e., the enhancement of the backward-angle cross section at higher energies through the u -channel contribution. The resonance currents can also interfere destructively with the nucleonic current in which case one obtains a larger $N\bar{N}^0$ coupling constant. In fact, in a very extreme case, we have obtained a t value as large as $g_{NN} = 3.0$. It is obvious, therefore, that a more unambiguous extraction of this coupling constant requires going to an energy region where the resonance contributions are small. Figure 8 illustrates this point; here we show the t result considering the data with energies at $T = 2.129$ GeV and above only and assuming a scenario in which no resonance currents contribute at these energies. The resulting t parameters are $g_{NN} = 2.28$ for the $N\bar{N}^0$ coupling constant and $v = 1257$ MeV for the cut parameter in the form factor at the \bar{N}^0 vertex. In Fig. 8 we see that the nucleonic and mesonic currents interfere with each other. However, the interference pattern is such that it does not cause any problem in xing both the nucleonic and mesonic current contributions to a large extent. In any case, judging from the overall results of our analysis, we would not expect g_{NN}^0 to be much larger than 2.

D. Spin observables

We now turn our attention to spin observables. As we have shown in Fig. 2, cross sections do not impose very severe constraints on the model parameter values. We expect spin observables to be more sensitive in this respect. The predictions for the beam and target asymmetries corresponding to the t results of Tables I–IV are shown in Fig. 9. As we can see, unlike the cross sections (see Fig. 2), the predictions vary considerably between the different parameter sets. For energies where the beam asymmetry is less sensitive to the parameter sets, the target asymmetry is quite sensitive and vice versa. Therefore, overall, a combined analysis of these spin observables will impose much more stringent constraints on the t and should help pin down the model parameters.

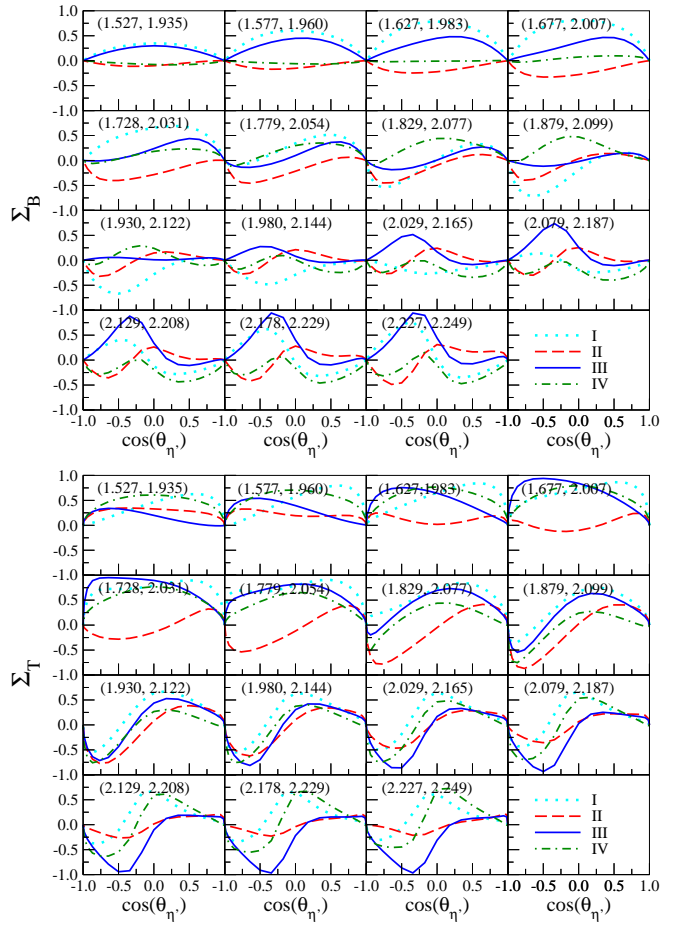


FIG. 9: (Color online) Photon beam and target nucleon asymmetries Σ_B (top panel) and Σ_T (bottom), respectively, for $p^+ p^0$ as a function of the \bar{N}^0 emission angle θ in the center-of-mass system. See the caption of Fig. 2 for the meaning of the different curves.

IV. SUMMARY

We have analyzed the new CLAS [9] data of the $p^+ p^0$ reaction within an approach based on a relativistic meson-exchange model of hadronic interactions. The present model is an extension of the one reported in Ref. [8] and it includes the nucleonic and the mesonic as well as the nucleon-resonance currents. The latter includes both spin-1/2 and -3/2 resonance contributions in contrast to our previous work [8], where only spin-1/2 resonances were considered. In addition, we employ energy-dependent resonance widths in the present work. The resulting reaction amplitude is fully gauge invariant.

We have shown that the mesonic as well as the spin-1/2 and -3/2 resonance currents are important to describe the existing data quantitatively. The observed angular distribution is due to delicate interference effects between the different currents. In our analysis, most of the resulting resonances may be identified with known resonances [18]. We emphasize, however, that one should be

cautious with such an identification of the resonances. As we have seen, the cross-section data alone do not impose enough constraints for an unambiguous determination of the resonance parameters. In this connection, we have shown that the beam and target asymmetries can help impose more stringent constraints. Furthermore, there is a possibility that some of the resonances in the present work are masking up background contributions, especially those due to the Δ -state interaction, which is not taken into account explicitly in our calculation. Obviously, effects of the Δ -state interaction should be investigated in future work before a conclusive identification of the resonances can be made.

Our study also shows that the nucleonic current should be relatively small. However, contrary to the expectation in our earlier work [8], the new high-precision cross-section data do not allow to pin down this current contribution due to the possible presence of resonance currents, especially of the D_{13} resonance, which can also lead to an enhancement of the cross section for backward angles at higher energies, a feature that otherwise arises from the u -channel nucleonic current contribution. It still remains to be corroborated whether the data at energies beyond the resonance region can, indeed, pin down the nucleonic current contribution. In any case, we would not expect the $N\bar{N}^0$ coupling constant to be much larger than $g_{NN^0} = 2$.

In this respect, it should be noted that the result pertaining here to the $N\bar{N}^0$ coupling constant is, of course, a model-dependent one. Indeed, what is relevant in our calculations is the product of g_{NN^0} and the associated hadronic form factor which accounts for the on-shellness of the intermediate nucleon. Moreover, our $N\bar{N}^0$ coupling constant is defined at the on-mass-shell point, i.e., $g_{NN^0} = g_{NN^0}(q^2 = m^2)$ while the coupling required in Eq. (1) in connection with the origin of the nucleon spin is at $q^2 = 0$. Since the 0 meson is a relatively heavy meson ($m \approx 957$ MeV), we would expect that $g_{NN^0}(q^2 = 0)$ will be considerably smaller than its value at $q^2 = m^2$, because of the presence of the form factor which usually cuts down the coupling strength. Therefore, we might well expect that the $N\bar{N}^0$ coupling at $q^2 = 0$ to be negligibly small, consistent with zero.

We have also shown that the mesonic current contribution cannot be fixed unambiguously from the existing cross-section data because of the possible presence of the resonance currents, especially the D_{13} resonance. A possibility to determine the t -channel current is to measure the cross sections at higher energies where the resonance contributions becomes negligible.

Finally, the results of the present work should provide useful information for further investigations, both experimentally and theoretically, of the $N^+ N^0$ reaction. In particular, it is imperative that spin observables such as the beam and target asymmetries be measured in order to learn more about the nucleon resonances in the energy region covered by the existing data. From the theoretical side, it is possible that the nucleon resonances introduced

in the present work are masking up the background contributions not taken into account in the calculation. In this connection, it is extremely interesting to investigate effects of the Δ -state interaction which has not been treated explicitly in the present calculation. Unfortunately, at present no realistic model is available that can provide the relevant $N\bar{N}$ Δ -state interaction. In addition, effects of higher-spin resonances that have been ignored in the present analysis should be investigated in the future.

Acknowledgments

The authors thank M. Dugger, B.G. Ritchie, and the CLAS Collaboration for providing the 0 data prior to publication. This work was supported by the COSY Grant No. 41445282 (COSY-58).

APPENDIX A : SPIN-3/2 RESONANCE PROPAGATOR

We employ here the Rarita-Schwinger (RS) choice for the free Lagrangian of a spin-3/2 particle with mass m ,

$$L = \dots ; \quad (A1)$$

where

$$= \frac{i}{2} [\dots ; (p + m)]_+ ; \quad (A2)$$

with $p = i\partial$, the anticommutator bracket $[a;b]_+ = ab + ba$, and $= \frac{i}{2} (\dots)$. (In the RS choice, the parameter A that usually appears in L is taken as $A = 1$ [19].) From

$$S = S = g ; \quad (A3)$$

the propagator is then found as

$$S(p) = \frac{(p + m)}{p^2 - m^2} = \frac{\sim (p + m)}{p^2 - m^2} ; \quad (A4)$$

where \sim is the RS tensor of Eq. (7) (with $m = m_R$) and

$$\sim = g + \frac{1}{3} + \frac{2p \cdot p}{3m^2} - \frac{p \cdot p}{3m} ; \quad (A5)$$

which differs from (7) by the sign of the last term.

When seeking an ansatz for describing a spin-3/2 resonance, we note first that there are, of course, ininitely many ways to achieve a pole description whose on-shell behavior on the real axis corresponds to replacing the mass of the elementary propagator by

$$m \rightarrow m_R - i\frac{R}{2} ; \quad (A6)$$

where m_R is the resonance mass and ${}_R$ the associated width. In constructing a resonant propagator, we are guided by the following motivation. As in the spin-1/2 case of (5), we want to describe the spin in terms of the elementary operators, i.e., we want to preserve the numerator structure of (A 4) and the symmetry between the RS tensors and $\tilde{\cdot}$. In a schematic matrix notation, we therefore make the ansatz

$$S = X^{-1} (\not{p} + m) = \tilde{(\not{p} + m)} X^{-1} ; \quad (A 7)$$

putting, in analogy to the denominator of the spin-1/2 case (5),

$$X = (\not{p}^2 - m_R^2)g + iA(\not{p} + m_R) ; \quad (A 8a)$$

$$X' = (\not{p}^2 - m_R^2)g + i(\not{p} + m_R)A' ; \quad (A 8b)$$

with the operators A and A' to be determined such that the second equality in (A 7) holds true, i.e.,

$$X^{-1} (\not{p} + m) = \tilde{(\not{p} + m)} X^{-1} ; \quad (A 9)$$

Multiplying this equation by \not{p} from both sides, one immediately finds the condition

$$(\not{p} + m_R)A' = A(\not{p} + m_R) ; \quad (A 10)$$

In view of Eq. (A 3) and the fact that on-shell, at $\not{p}^2 = m_R^2$ and acting on a spin-3/2 eigenstate, the propagator must provide the width information, we find that the ansatz

$$A' = \frac{1}{2} \quad \text{and} \quad A = \tilde{\frac{1}{2}} ; \quad (A 11)$$

satisfies all constraints. Here m may be any conveniently chosen width function that goes to the static width ${}_R$ at the resonance mass m_R . We thus have

$$S(\not{p}) = (\not{p} - m_R)g - i\frac{1}{2} ; \quad (A 12a)$$

or

$$S(\not{p}) = \tilde{(\not{p} - m_R)g} - i\frac{1}{2} ; \quad (A 12b)$$

By construction, both forms are completely equivalent, similar to the equivalence of both forms for the elementary propagator (A 4).

The inversion here is to be performed on the full 16-dimensional space of Lorentz indices and component indices. There are various equivalent ways to do this; we have done it by introducing indices

$$i = 4 + \quad \text{and} \quad j = 4 + ; \quad (A 13)$$

where $i = 0; 1; 2; 3$ are the Lorentz indices and $j = 1; 2; 3; 4$ are the component indices, and defining 16 16 numerator and denominator matrices by

$$\begin{aligned} N_{ij} &= g \\ &= \frac{2p \cdot p}{3m_R^2} \\ &+ \frac{1}{3} \not{p} \not{p} + \frac{p \not{p} \not{p}}{3m_R} g \end{aligned} ; \quad (A 14)$$

and

$$D_{ij} = p \not{p} m_R \not{p} + iN_{ij}\frac{1}{2} ; \quad (A 15)$$

respectively. Numerically inverting the denominator matrix D , we then calculate the spin-3/2 propagator as

$$S = D^{-1} N_{ik} g ; \quad (A 16)$$

where $k = 4 +$ and summation over i is implied, as usual.

[1] S. Capstick and N. Isgur, Phys. Rev. D 34, 2809 (1986); S. Capstick and W. Roberts, *ibid.* 47, 1994 (1993); 49, 4570 (1994); 57, 4301 (1998); 58, 074011 (1998).
[2] J. Ashman et al., Phys. Lett. B 206, 364 (1988).
[3] G. M. Shore and G. Veneziano, Nucl. Phys. B 381, 23 (1992).
[4] T. Hatsuda, Nucl. Phys. B 329, 376 (1990); A. V. Efremov, J. Soer, and N. A. Tomqvist, Phys. Rev. Lett. 64, 1495 (1990); Phys. Rev. D 44, 1369 (1991).
[5] G. M. Shore and G. Veneziano, Phys. Lett. B 244, 75 (1990).
[6] S. Okubo, Phys. Lett. 5, 165 (1963); G. Zweig, CERN Report No. TH 412, 1964; J. Iizuka, Prog. Theor. Phys. Suppl. 37{38}, 21 (1966).
[7] G. Altarelli and G. G. Ross, Phys. Lett. B 212, 391 (1988); R. D. Carlitz, J. C. Collins, and A. H. Müller, *ibid.* B 214, 229 (1988).
[8] K. Nakayama and H. Haberzettl, Phys. Rev. C 69, 065212 (2004).
[9] M. Dugger et al. (CLAS collaboration), in preparation.
[10] R. P. Borchert et al., Phys. Lett. B 444, 555 (1998); J. Barth et al., Nucl. Phys. A 691, 374c (2001).
[11] H. Haberzettl, Phys. Rev. C 56, 2041 (1997).
[12] H. Haberzettl, C. Bennhold, T. Mart, and T. Feuster, Phys. Rev. C 58, R 40 (1998).
[13] R. M. Davidson and R. W. Orkman, Phys. Rev. C 63, 025210 (2001).
[14] R. L. Walker, Phys. Rev. 182, 1729 (1969).
[15] R. A. Amid, R. L. Walker, Z. Li, and L. D. Roper, Phys. Rev. C 42, 1864 (1990).
[16] A. I. L'vov, V. A. Petrun'kin, and M. Schumacher, Phys. Rev. C 55, 359 (1997).

- [17] D. D rechsel, O. H anstein, S.S. K am alov, and L. T iator, Nucl. Phys. A 645, 145 (1999) [nucl-th/9807001].
- [18] Particle D ata G roup, Phys. Lett. B 592, 1 (2004).
- [19] P.A. M oldauer and K.M. C ase, Phys. Rev. 102, 279 (1956); C. F ronsdal, Nuovo C imento Suppl. 9, 416 (1958); A. A urelia and H. Umezawa, Phys. Rev. 182, 1682 (1969); L.M. N ath, B. E tem adi, and J.D. K in el, Phys. Rev. D 3, 2153 (1971); M. B enm errouche, R.M. D avidson, and N.C. M ukhopadhyay, Phys. Rev. C 39, 2339 (1989).